Supporting Information

Homologous Heterostructures of Ni/NiFeO Mott-Schottky for Alkaline Water Electrolysis

Manna Liu[1,2#], Hua Yang[1,2#], Zihao Zhou[2], Yingxia Zhao[2], Jinkai Yuan[4], Shaomin Peng[1,2*], Ming Sun[1,2,3*], Lin Yu[1,2*]

[1] Jieyang Branch of Chemistry and Chemical Engineering Guangdong Laboratory (Rongjiang Laboratory), Jieyang 515200, China

[2] GuangDong Engineering Technology Research Center of Modern Fine Chemical Engineering, School of Chemical Engineering and Light Industry, Guangdong University of Technology, 510006 Guangzhou, P. R. China

[3]Guangdong Yuntao Hydrogen Energy Technology Co., Ltd, 551040 Guangzhou, China

[4]Centre de Recherche Paul Pascal, CNRS, University of Bordeaux, UMR5031, 115 Avenue Schweitzer, 33600, Pessac, France

1 Experimental

1.1 Chemicals.

$Ni(NO_3)_2 \cdot 6H_2O$, $Fe(NO_3)_3 \cdot 9H_2O$, $C_6H_{12}N_4$(Hexamethylenetetramine, HMT), CH_3OH(methanol), C_3H_6O (acetone), C_2H_5OH (ethanol) and hydrochloric acid (36.5% concentration) are from Guangzhou Chemical Reagent Factory with AR grade. Fe foam is from Shanghai Hesen Co. KOH is from Shanghai Aladdin Biochemical Technology Co. with Electronics grade (99.999%).

1.2 Characterization

X-ray diffraction (XRD) analysis was performed using PANalytical (X 'PerT3

[#] These two authors contribute equally.
* Corresponding author: smpeng0814@gdut.edu.cn; sunmgz@gdut.edu.cn; gych@gdut.edu.cn

Powder) and PANalytical (Aeris) type X-ray diffractometers equipped with Cu Kα radiation (40 kV, 44 mA) at a scanning speed of 5° min^{-1}. The morphology and size of the samples were observed using a SU8220 (Hitachi) cold field emission scanning electron microscope (SEM). Transmission electron microscopy (TEM) analyses were performed on a Talos F200S from the Czech FEI Company equipped with an energy dispersion spectrometer (EDS). X-ray photoelectron spectroscopy (XPS) was acquired on an Escalab 250Xi (Thermo Fisher, UK) using a monochromatic Al Kα source. The TG-FTIR-MS test was carried out in the combined system of thermogravimetric analyzer (Nicolet IS 50, Mettler Toledo), infrared spectroscopy instrument (Trace1300, Thermofisher), and mass spectrometry analyzer (ISQQD, Thermo Fisher) respectively. The inductively coupled plasma emission spectrometer (ICP) was tested by a spectrometer (Agilent, Model 720). Sample was first weigh and fully digested with acid, and then wait for the test. Ultraviolet photoemission spectroscopy (UPS) was conducted with a Thermo Fisher Scientific ESCALAB 250Xi and a VG Scienta R4000 analyzer (monochromatic He I light source of 21.22 eV). The formula $\varphi = h_v - E_{cutoff}$ is used to calculate the work function (φ), reflecting the electron dynamics on the sample surface, where h_v represents the energy of the incident photon (21.22 eV), and E_{cutoff} is obtained by normalizing quadratic electron cutoff spectrum.

1.3 Electrochemical activity test

All electrochemical measurements were performed in a three-electrode system at Zennuim Electrochemical workstation (Zahner, Zennuim), with Ni/NiFeO/FF as the direct working electrode, graphite rod as the counter electrode, and Ag/AgCl (3.5 M KCl, 0.2046 V vs. RHE) as the reference electrode. The HER test was performed in N2 saturated 1.0 M KOH aqueous solution, and the OER test was performed in O2 saturated solution. Ni/NiFeO/FF was used as anode and cathode in the double electrode electrolytic cell to test the total hydrolysate. The measured potential has been converted to the potential relative to the reversible hydrogen electrode (RHE), and the following formula is used to convert the potential:

$$E_{RHE} = E_{Ag/AgCl} + 0.059pH + E°_{reference\ voltage}\ (pH \approx 14).$$

The polarization curves of the catalysts were recorded by Linear Sweep Voltammetry (LSV) at a scanning rate of 1 mV s^{-1}. All polarization curves were corrected with 95% IR compensation. Cyclic voltammetry (CV) was used to measure the double layer capacitance (C_{dl}) of the catalyst in the non-Faraday interval at different sweep speeds. The electrochemical active surface area (ECSA) of the catalyst can be calculated according to the double layer capacitance (C_{dl}), and the formula is ECSA=C_{dl}/C_s, C_s refers to the specific capacitance of the sample under the same electrolyte condition. According to existing reports, C_s=0.040 mF cm^{-2} is usually selected under the test condition of 1M KOH electrolyte. Electrochemical impedance spectroscopy (EIS) was performed by applying the potential corresponding to 10mA cm^{-2} according to LSV curve in the frequency range of 100 kHz ~ 0.01 Hz. The Faraday efficiency of the reaction between HER and OER was determined by gas chromatography. The stability of the catalyst was investigated by comparing the changes of LSV curve before and after 1000 cycles of CV aging, or by observing the changes of overpotential during constant current measurement. In addition, different current densities were applied to test the material at constant current to explore the electrochemical stability of the material in practical applications.

Faraday efficiency (FE) is measured by Gas Chromatography. Firstly, at least three different concentrations of hydrogen (oxygen) are prepared in the air bag respectively and injected into the Gas Chromatography analyzer to obtain the standard curve of the two gases. Then, the gas produced by HER (OER) reaction in different time periods (15min, 20min, 25min, 30min, 40min) was collected with a 5ml sampler with good air tightness. The concentration of the gas can be obtained by injecting the gas into a gas chromatography analyzer for analysis.

The Faraday efficiency (FE) can be calculated by the following formula:

$$FE = \frac{\quad}{,} \quad ,$$

Where C is the measured gas concentration; V is the volume of the gas in the electrolytic cell; Z is the number of electrons transferred during the reaction, in hydrogen evolution and oxygen evolution reaction, Z is equal to 2 and 4, respectively;

F is Faraday constant (96485.3383±C/mol) and Q is the electric flux during the reaction time.

1.4 DFT computation details

The calculations were carried out using density functional theory with the PBE form of generalized gradient approximation functional (GGA) [1]. The Vienna ab-initio simulation package (VASP) [2,3,4,5] was employed. The plane wave energy cutoff was set as 400 eV. The Fermi scheme was employed for electron occupancy with an energy smearing of 0.1 eV. The first Brillouin zone was sampled in the Monkhorst−Pack grid[6]. The 3×3×1 k-point mesh for the surface calculation. The energy converged to 1.0×10^{-5} eV/atom and the force converged to 0.01eV/Å were set as the convergence criterion for geometry optimization. In structural optimization calculations, the most bottom layer of atoms was fixed, and other layers of atoms were allowed to relax. A vacuum layer as large as 15 Å was used along the c direction normal to the surface to avoid periodic interactions. The (004) surface is cut from the bulk $Ni_3Fe_1O_4$ according to XRD. To model the $Ni_3Fe_1O_4$ loaded Ni nanoparticle catalyst, a Ni cluster with six Ni atoms were chosen. For OER, The Gibbs free-energy change (ΔG_{ads}) of adsorbed intermediates on the catalysts is defined as follows:

$$\Delta G_{ads} = \Delta E_{ads} + \Delta E_{ZPE} - T\Delta S$$

where ΔE_{ads} is the adsorption energy of intermediates on the catalysts, ΔE_{ZPE} is the zero-point energy correction. ΔS is the entropy correction.

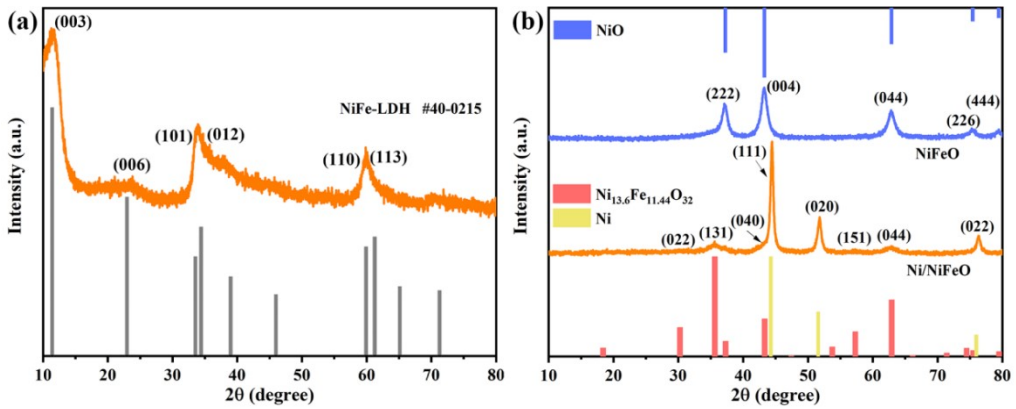

Fig.S1 XRD patterns of (a) NiFe-LDH and (b)NiFeO and Ni/NiFeO

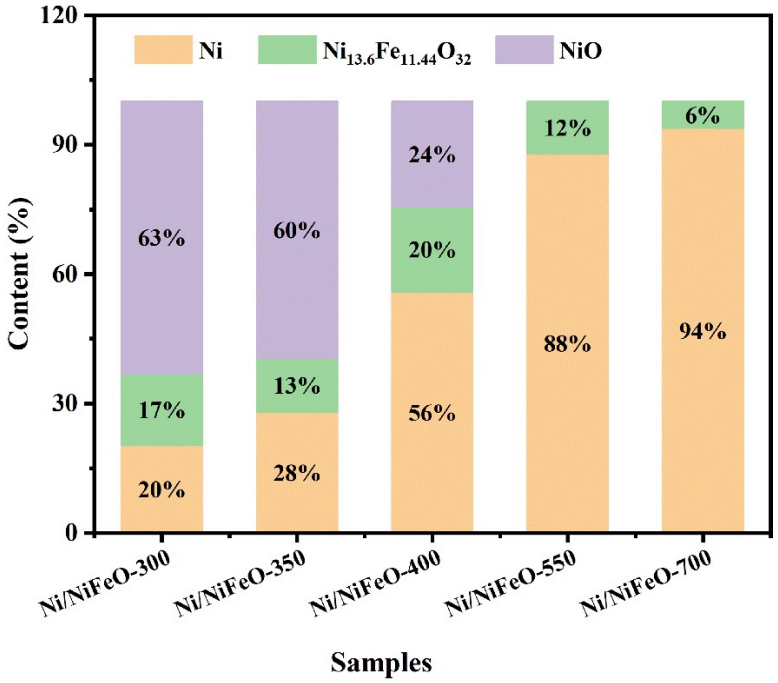

Fig.S2 Phase content of catalysts obtained by roasting NiFe-LDH precursors at different temperatures from 25~700 °C

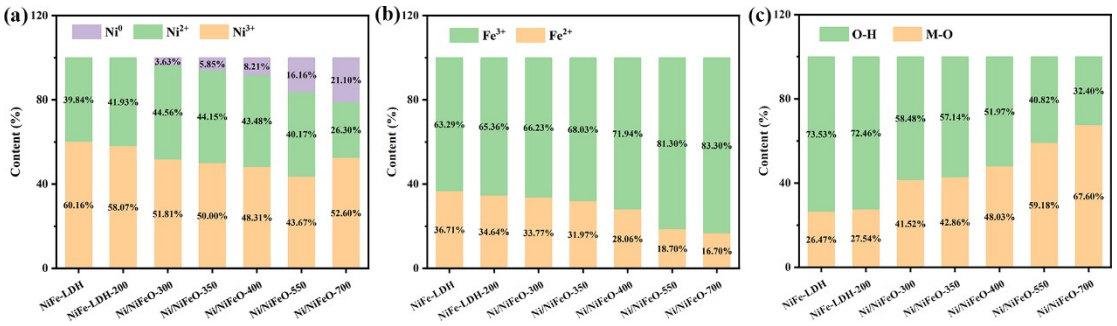

Fig.S3 XPS peak fitting result: (a)Ni 2p, (b) Fe 2p and (c) O 1s of Different catalysts

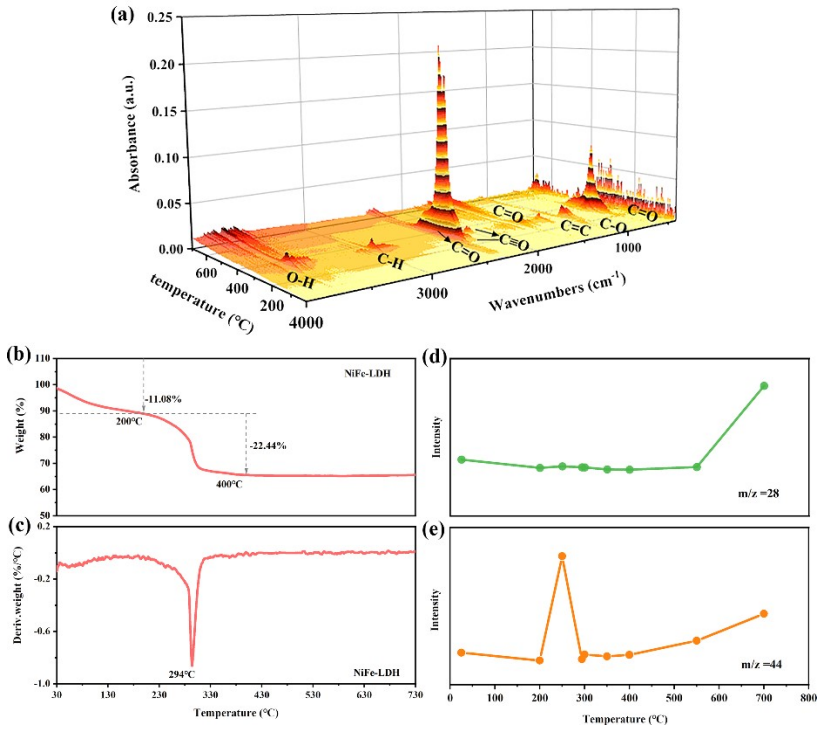

Fig.S4 (a) TG-FTIR spectra ;(b-c) TG-DTG curves; curves of gaseous decomposition products (d)m/z=28, CO; (e)m/z=44, CO_2 derived from pyrolysis process tracking by TG-MS.

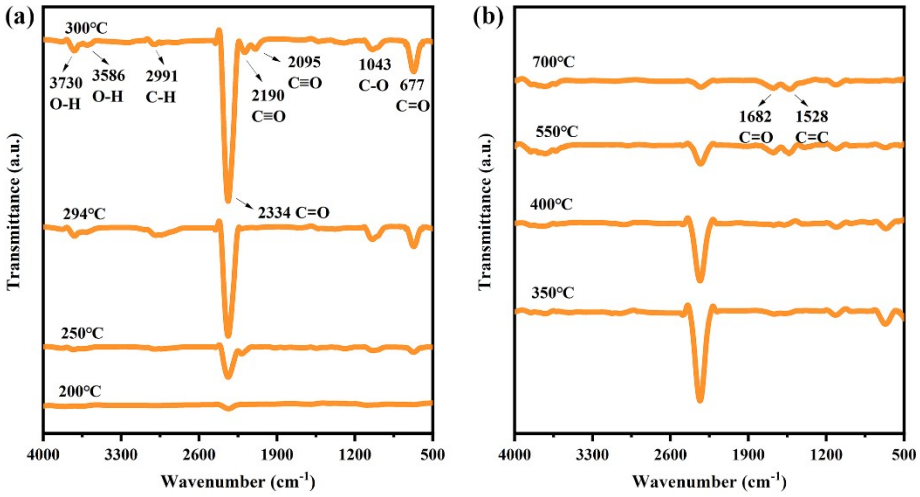

Fig.S5 FTIR spectra of NiFe -LDH pyrolysis at (a)200-300 °C；(b)350-700 °C based on TG-FTIR spectra data；

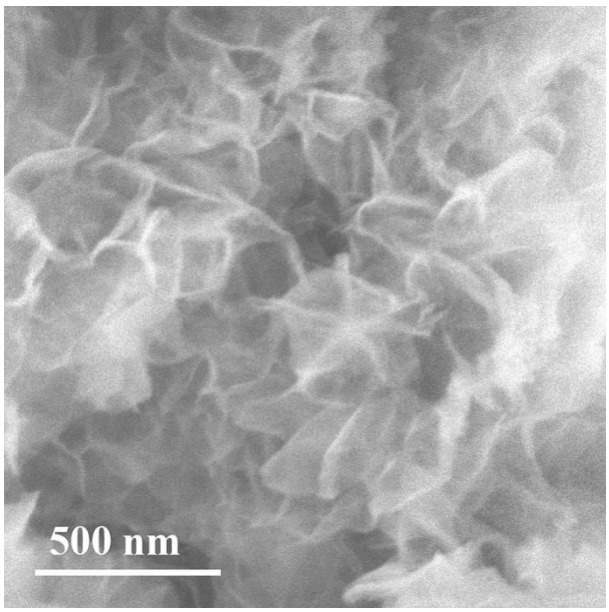

Fig.S6 SEM images of precursor NiFe-LDH.

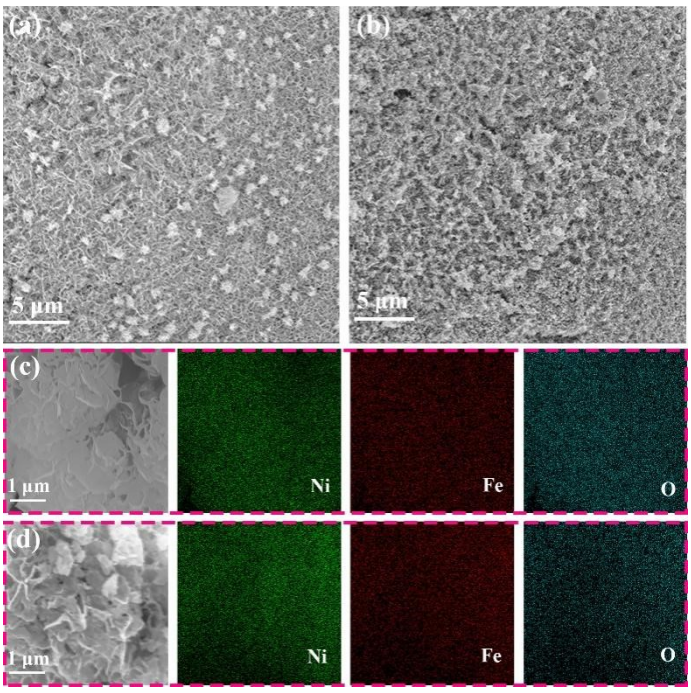

Fig.S7 Low resolution SEM images of (a) NiFeO and (b) Ni/NiFeO; STEM energy-dispersive X-ray (EDX) spectroscopy elemental mapping of (c) NiFeO and (d) Ni/NiFeO.

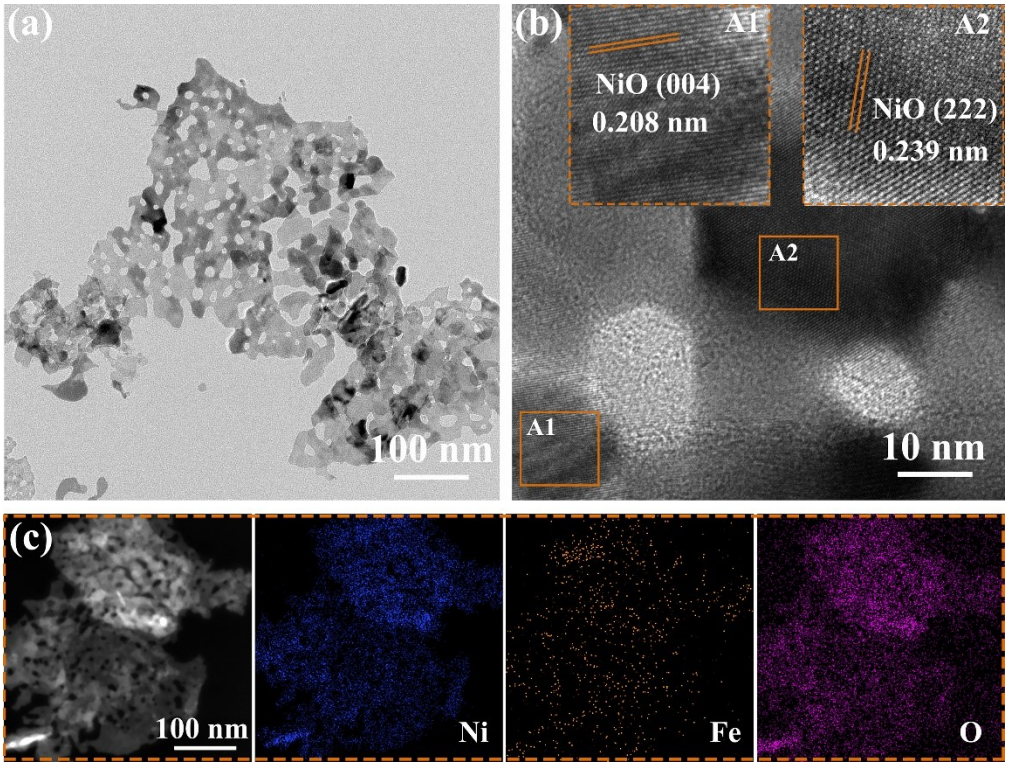

Fig.S8 (a) TEM images and (b) HRTEM images of NiFeO; (c) HAAD-STEM image and associated elemental mapping images.

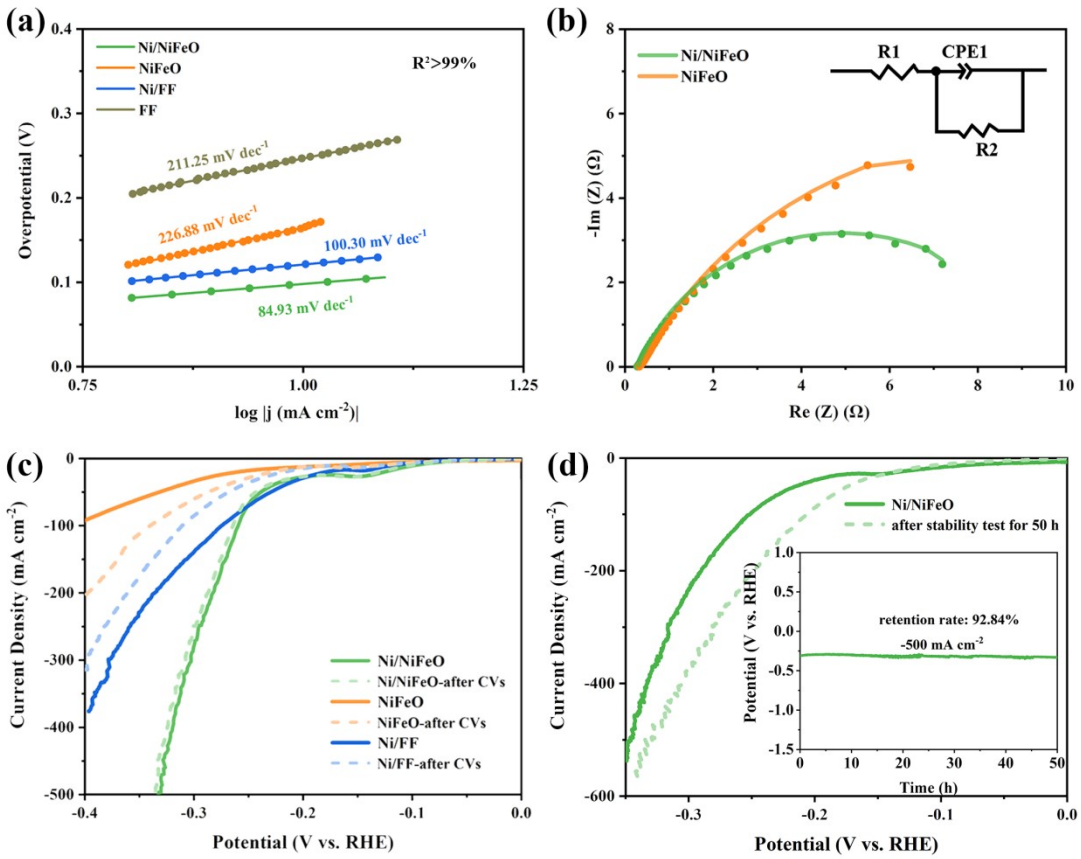

Fig.S9 HER performance in 1.0 M KOH: (a) Tafel plots; (b) Nyquist plots; (c) polarization curves before and after 1000 cycles of CV under the scan rate of 100 mV s^{-1}; (d) v-t curves at -500 mA cm^{-2} for 50 h and LSV curve before and after the test.

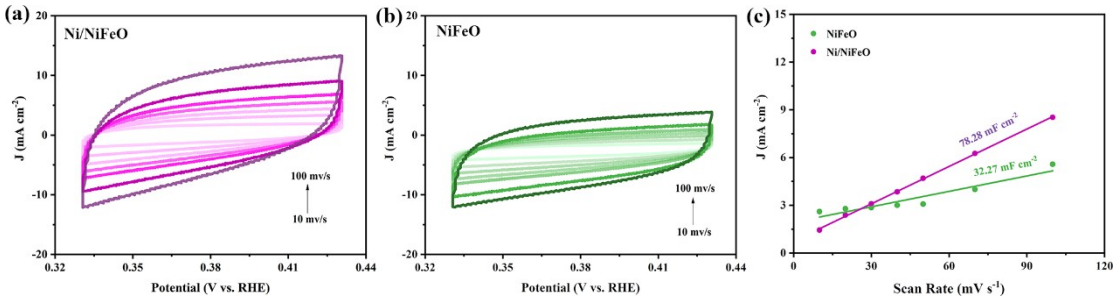

Fig.S10 Typical cyclic voltammetry curves of (a) Ni/NiFeO and (b) NiFeO electrodes in 1 M KOH at scan rates ranging from 10 to 100 mV s^{-1}; (c) The double layer capacitance of both (C_{dl})

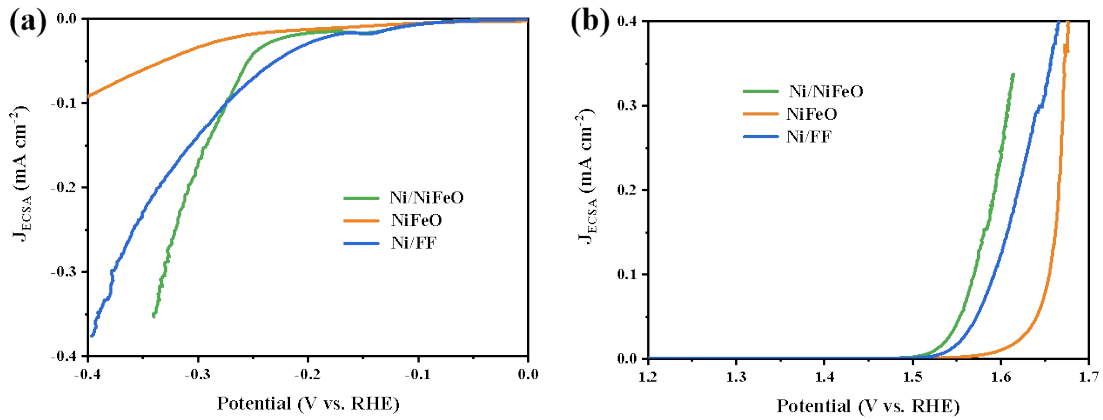

Fig. S11. ECSA-normalized LSV curves: (a) HER; (b) OER

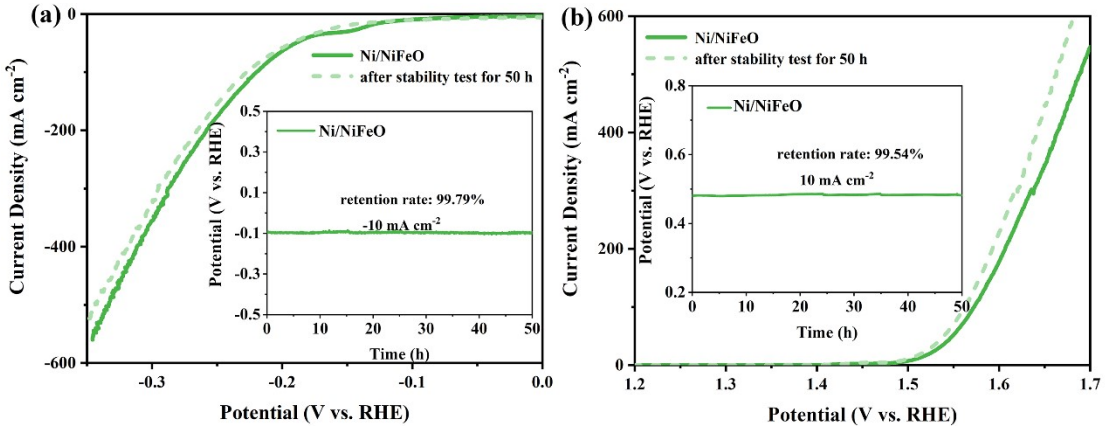

Fig.S12 v-t curves at 10 mA cm^{-2} for 50 h and LSV curve before and after the (a)HER and (b)OER test.

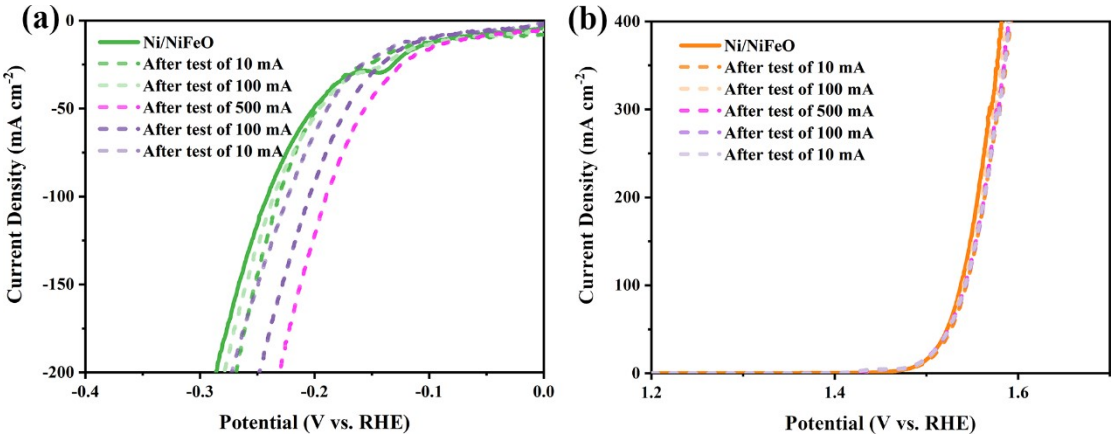

Fig.S13 LSV curve after (a)HER and (b)OER test at different current densities (from 10 mA cm^{-2}→100 mA cm^{-2}→500 mA cm^{-2}→100 mA cm^{-2}→10 mA cm^{-2})

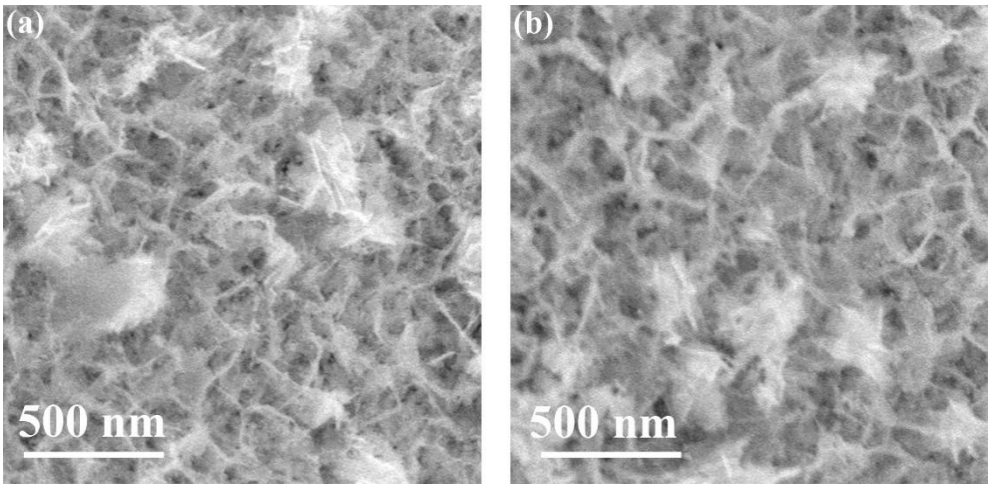

Fig.S14 SEM images of Ni/NiFeO after (a)HER and (b)OER stability test.

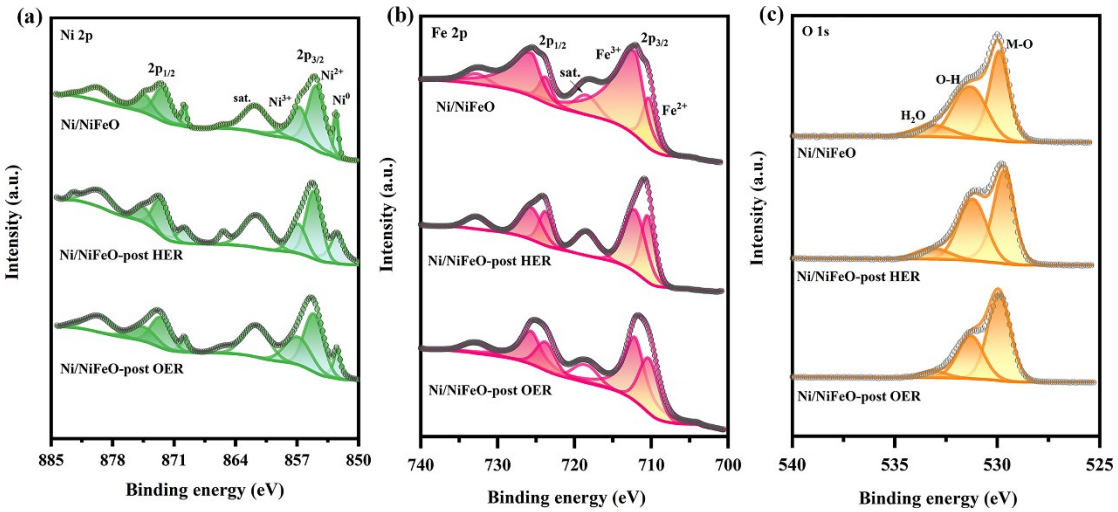

Fig.S15 High-resolution XPS spectra of Ni/NiFeO after HER and OER stability test: (a) Ni 2p, (b) Fe 2p, (c) O 1s.

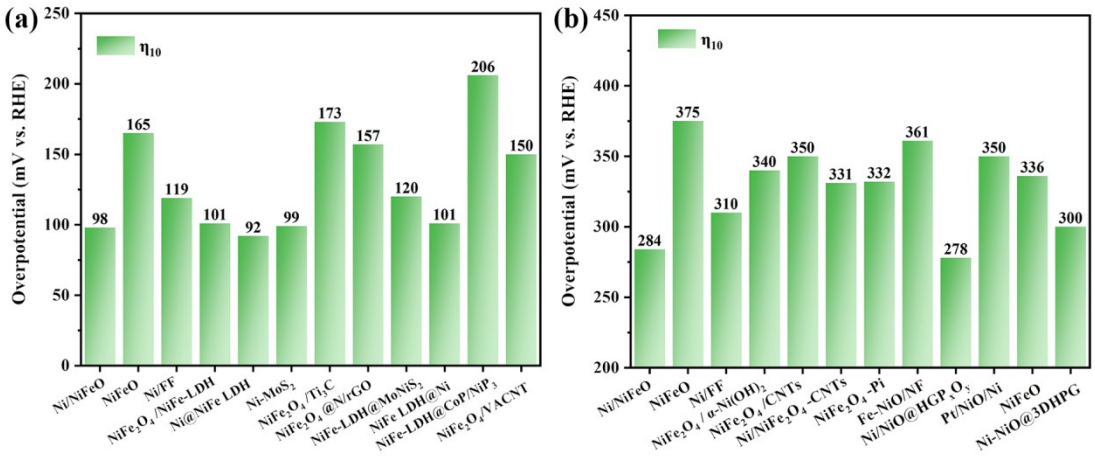

Fig.S16 (a) the overpotential at 10 mA cm^{-2} for Ni/NiFeO with other HER catalysts (η-10) ; (b) the overpotential at 10 mA cm^{-2} for Ni/NiFeO with other OER catalysts (η10)

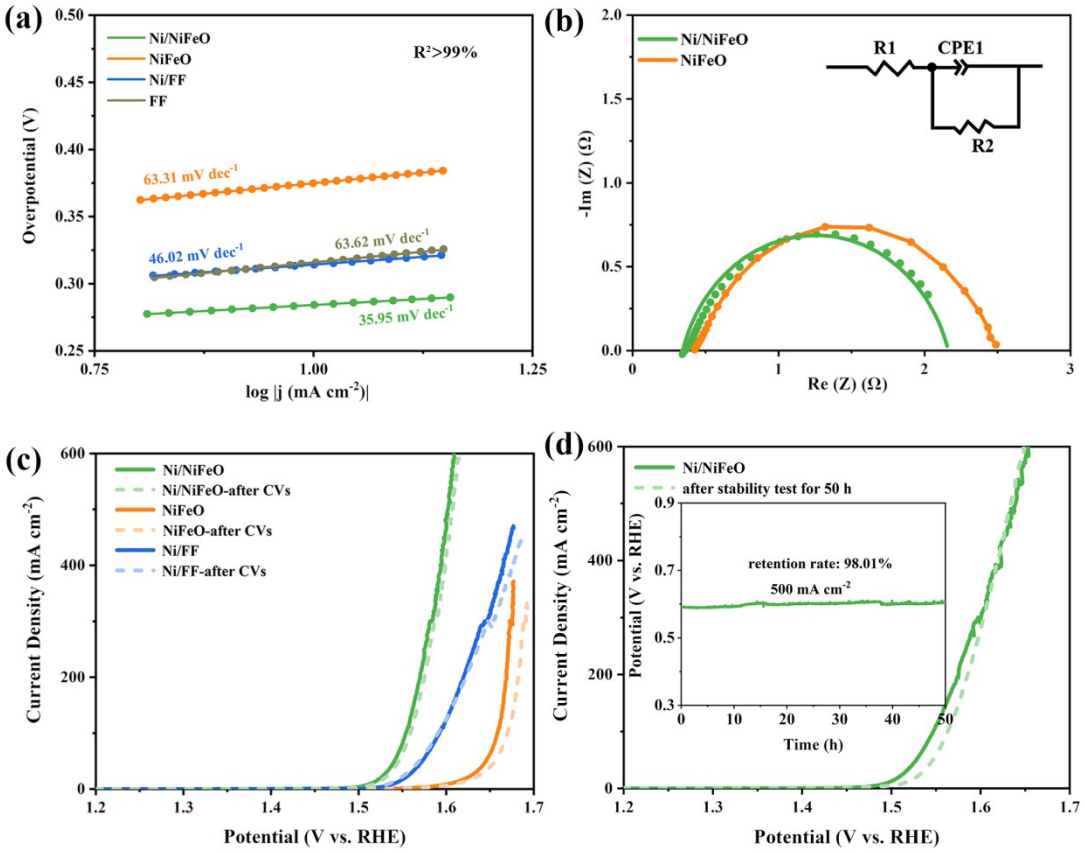

Fig.S17 OER performance in 1.0 M KOH: (a) Tafel plots; (b) Nyquist plots; (c) polarization curves before and after 1000 cycles of CV under the scan rate of 100 mV s^{-1}; (d) v-t curves at -500 mA cm^{-2} for 50 h and LSV curve before and after the test.

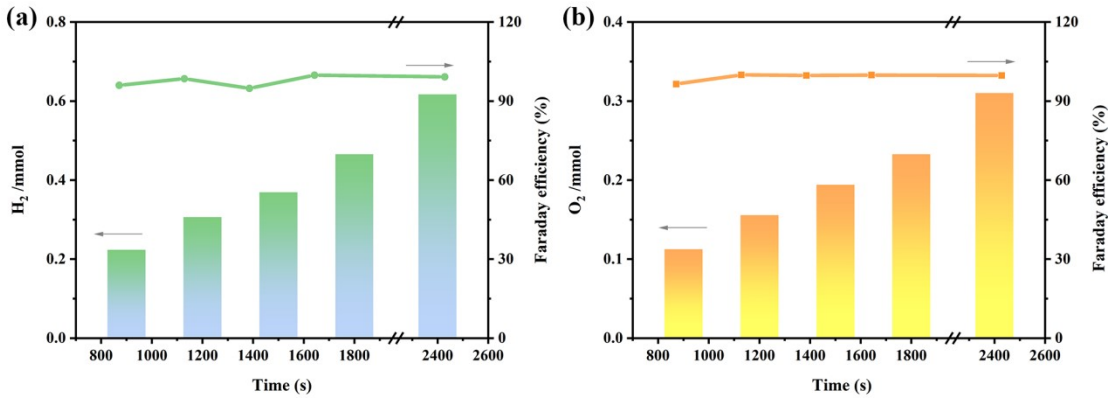

Fig.S18 Faraday efficiency in (a) HER and (b) OER processes

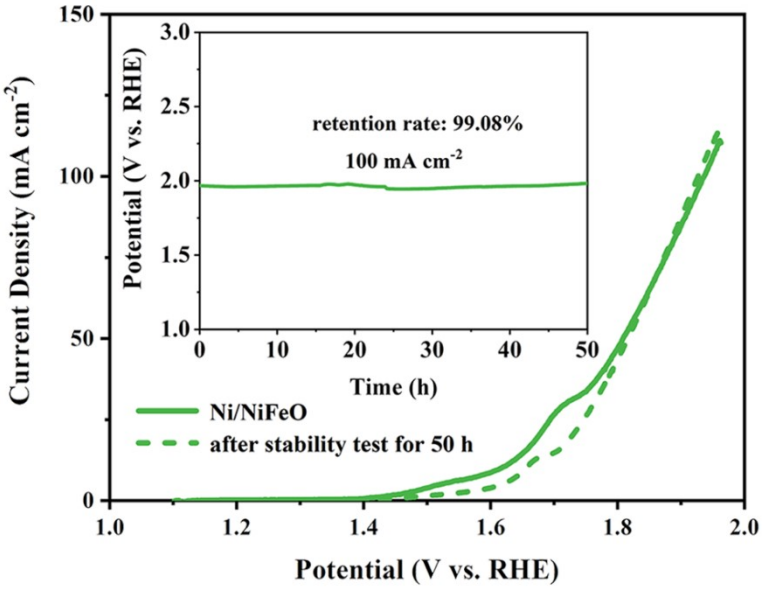

Fig.S19 Long-term stability at 100 mA cm^{-2} of overall water-splitting using Ni/NiFeO as both anode and cathode electrocatalysts in a two-electrode system

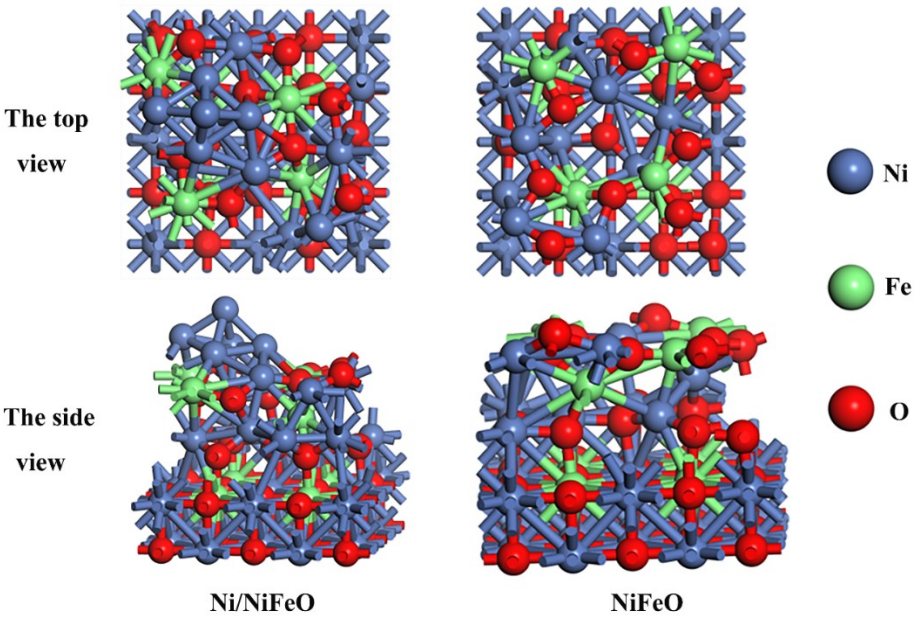

Fig.S20 The top view and side view of models of Ni/NiFeO and NiFeO.

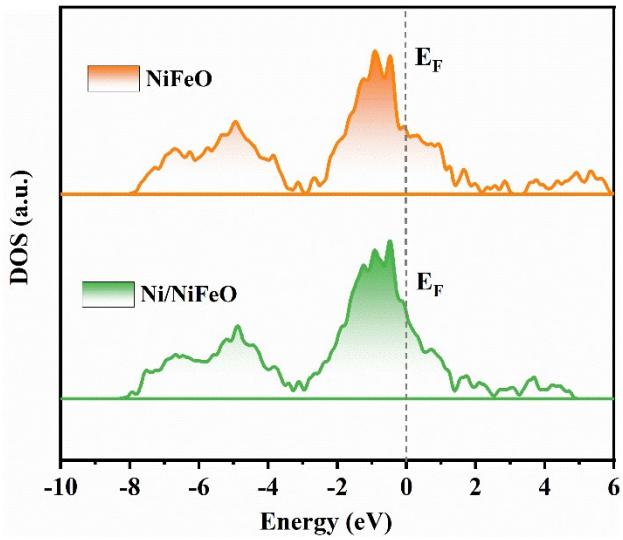

Fig.S21 density of states (DOS) plots of Ni/NiFeO.

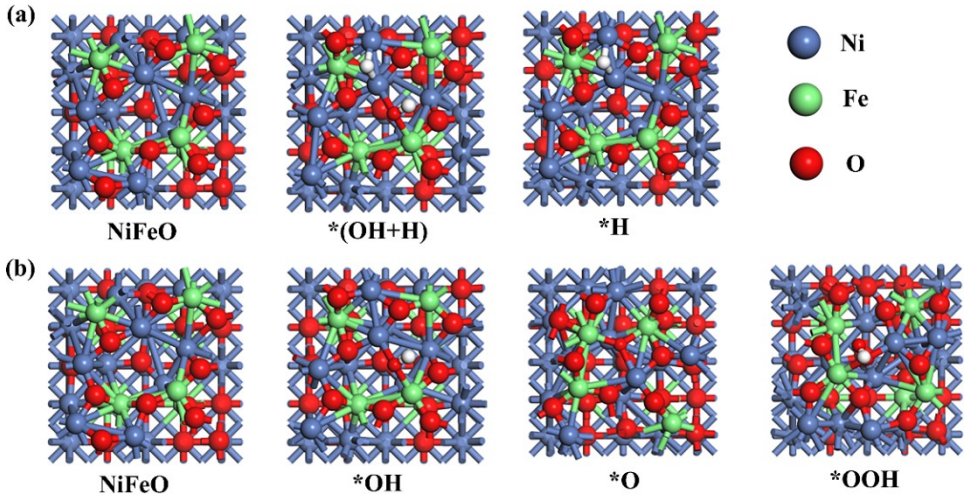

Fig.S22 The structure of the intermediates adsorbed on the NiFeO catalyst surface during the (a)HER and (b)OER process.

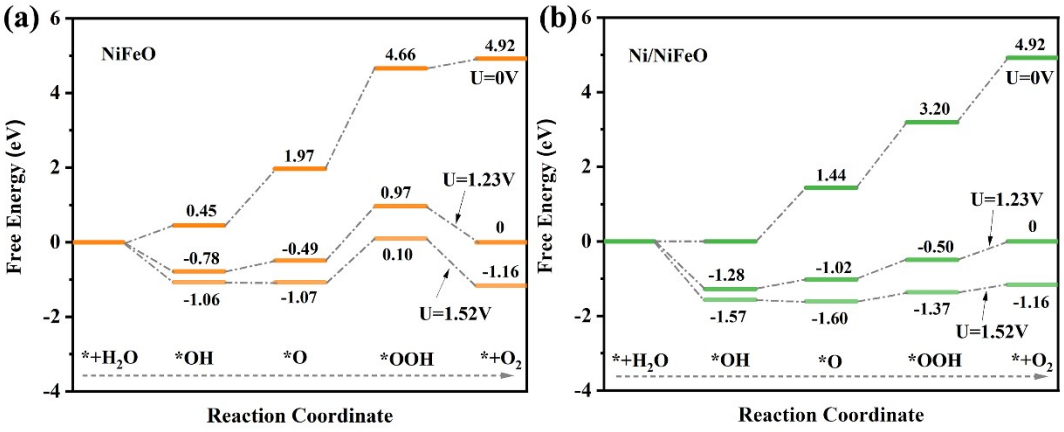

Fig.S23 The free energy diagram for OER steps (from left to right) at different applied potentials (U, vs.RHE) of (a) NiFeO and (b) Ni/NiFeO.

Table S1 XPS peak fitting result

	Ni2p			Fe2p		O1s	
	Ni^0	**Ni^{2+}**	**Ni^{3+}**	**Fe^{2+}**	**Fe^{3+}**	**M-O**	**O-H**
NiFeO	---	0.606	0.394	0.333	0.667	0.746	0.254
Ni/NiFeO	0.162	0.402	0.436	0.187	0.813	0.592	0.408
Ni/NiFeO -post HER	0.263	0.505	0.232	0.398	0.602	0.541	0.459
Ni/NiFeO -post OER	0.138	0.513	0.349	0.367	0.633	0.645	0.355

Table S2 Comparison of the HER activity of the Ni/NiFeO with other recently reported metal-based HER electrocatalysts in basic condition.

Catalyst	**Electrolyte**	**Substrate**	**η for HER @ corresponding j (mV@ mA cm^{-2})**	**References**
Ni/NiFeO	1M KOH	Fe foam	98@10 259@100	This work
NiFeO	1M KOH	Fe foam	165@10 411@100	This work
Ni/FF	1M KOH	Fe foam	119@10 274@100	This work
$NiFe_2O_4$ /NiFe LDH	1M KOH	Ni foam	101@10	7
Ni@NiFe LDH	1M KOH	Ni foam	92@10	8
Ni-MoS_2	1M KOH		99@10	9
$NiFe_2O_4$ /Ti_3 C	1M KOH	Ni foam	173@10	10
$NiFe_2O_4$ @N/rGO	1M KOH	Ni foam	157@10	11
NiFe-LDH@MoNiS_2	1M KOH	Ni foam	120@10	12
NiFe LDH@Ni NTAs/NF	1M KOH	Ni foam	101@10	13
NiFe-LDH @CoP/NiP_3	1M KOH	Ni foam	206@50	14
$NiFe_2O_4$/VA CNT	1M KOH	Ni foam	150@10	15

Table S3 Comparison of the OER activity of the Ni/NiFeO with other recently reported metal-based OER electrocatalysts in basic condition.

Catalyst	**Electrolyte**	**Substrate**	**η for OER @ corresponding j (mV@ mA cm^{-2})**	**Reference**
Ni/NiFeO	1M KOH	Fe foam	284@10 324@100	This work
NiFeO	1M KOH	Fe foam	375@10 428@100	This work
Ni/FF	1M KOH	Fe foam	310@10 362@100	This work
$NiFe_2O_4$ / α-$Ni(OH)_2$	1M KOH	glassy carbon	340@10	16
$NiFe_2O_4$ /CNTs	1M KOH	Ni foam	350@10	17
Ni/$NiFe_2O_4$ -CNTs	1M KOH	glassy carbon	331@10	18
$NiFe_2O_4$ -Pi	1M KOH	glassy carbon	332@10	19
Fe-NiO/NF	1M KOH	Ni foam	361@10	20
Ni/NiO@HGP $_xO_y$	1M KOH	glassy carbon	278@10	21
Pt/NiO/Ni	1M KOH	glassy carbon	350@10	22
NiFeO	1M KOH	Carbon Cloth	336@10	23
Ni-NiO @3DHPG	1M KOH	glassy carbon	300@10	24

Table S4 Comparison of the overall water splitting of the Ni/NiFeO with other recently reported metal-based bifunctional electrocatalysts

Catalyst	**Electrolyte**	**Substrate**	**η for overall water splitting @ corresponding j (V@ mA cm^{-2})**	**Reference**
Ni/NiFeO	1M KOH	Fe foam	1.60@10	This work
CoNiP/MP Ni	1M KOH	micro-sized porous nickel substrate	1.66@10	25
CoP–N /Co foam	1M KOH	Co foam	1.61@10	26
Co_xP–Fe_2P /NF	1M KOH	Ni foam	1.605@10	27
NiFeCoPi/P @SSFF	1M NaOH + 0.5 M Na_2CO_3 /$NaHCO_3$	Stainless steel fiber felt	1.63@10	28
CoCr-LDH/ NiO/NF	1M KOH	Ni foam	1.57@10	29
Fe-Ni_2P/Ni_5P_4@ NC	1M KOH	Ni foam	1.56@10	30
NixCoyP /Co_2P@NF	1M KOH	Ni foam	1.75@100	31
C@CoP-FeP /FF	Simulated sea water	Fe foam	1.70@100	32

Reference

1. J. P. Perdew, K. Burke and E. M., *PHYSICAL REVIEW LETTERS*, 1996, **77**, 3865-
2. 3868 Kresse and J. Furthmüller, *Comp. Mater. Sci*, 1996, **6**, 15-50.
3. G. Kresse and J. Hafner, *Phys Rev B Condens Matter*, 1993, **47**, 558-561.
4. G. Kresse and J. Hafner, *Phys Rev B Condens Matter*, 1994, **49**, 14251-14269.
5. G. Kresse and J. Furthmüller, *54*, 1996, 11169-11186.
6. H. J. Monkhorst and J. D. Pack, *Physical Review B*, 1976, **13**, 5188-5192.
7. Z. Wu, Z. Zou, J. Huang and F. Gao, *ACS Appl Mater Interfaces*, 2018, **10**, 26283-26292.
8. Z. Cai, X. Bu, P. Wang, W. Su, R. Wei, J. C. Ho, J. Yang and X. Wang, *Journal of Materials Chemistry A*, 2019, **7**, 21722-21729.
9. J. Zhang, T. Wang, P. Liu, S. Liu, R. Dong, X. Zhuang, M. Chen and X. Feng, *Energy & Environmental Science*, 2016, **9**, 2789-2793.
10. P. V. Shinde, P. Mane, B. Chakraborty and C. Sekhar Rout, *J Colloid Interface Sci*, 2021, **602**, 232-241.
11. L. Cao, Z. Li, K. Su, M. Zhang and B. Cheng, *J. Energy Chem.* , 2021, **54**, 595-603.
12. Y. Li, T. Dai, Q. Wu, X. Lang, L. Zhao and Q. Jiang, *Materials Today Energy*, 2022, **23**.
13. Y. Tang, Q. Liu, L. Dong, H. B. Wu and X.-Y. Yu, *Appl.Catal. B*, 2020, **266**.
14. C. Song, Y. Liu, Y. Wang, S. Tang, W. Li, Q. Li, J. Zeng, L. Chen, H. Peng and Y. Lei, *Science China Materials*, 2021, **64**, 1662-1670.
15. Y. Xu, Y. Yan, T. He, K. Zhan, J. Yang, B. Zhao, K. Qi and B. Y. Xia, *Carbon*, 2019, **145**, 201-208.
16. H. Chen, J. Yan, H. Wu, Y. Zhang and S. Liu, *Journal of Power Sources*, 2016, **324**, 499-508.
17. N. Xu, Y. Zhang, T. Zhang, Y. Liu and J. Qiao, *Nano Energy*, 2019, **57**, 176-185.
18. X. Yu, G. Chen, Y. Wang, J. Liu, K. Pei, Y. Zhao, W. You, L. Wang, J. Zhang, L. Xing, J. Ding, G. Ding, M. Wang and R. Che, *Nano Research*, 2020, **13**, 437-446.